Renewable Energy 187 (2022) 484–499

Contents lists available at ScienceDirect

Renewable Energy

journal homepage: www.elsevier.com/locate/renene

Designing a flat beam-down linear Fresnel reflector

Sebastián Taramona *, Pedro Ángel González-Gómez , Javier Villa Briongos , Jesús Gómez-Hernández

Universidad Carlos III de Madrid, Escuela Politécnica Superior. Department of Thermal and Fluid Engineering, Energy Systems Engineering Group (ISE). Av. Universidad 30, 28911, Leganés, Madrid, Spain

ARTICLE INFO

Article history:
Received 3 November 2021
Received in revised form
10 January 2022
Accepted 25 January 2022
Available online 29 January 2022

Keywords:
Beam-down linear Fresnel reflector
Flat secondary reflector
Solar field optimization
Flux concentration
Optical efficiency

ABSTRACT

A linear beam-down solar field consists of two reflections that concentrate the solar irradiation on heavy materials located on the ground. Several rows of linear Fresnel reflectors, which have the same width, aim the solar irradiation to a secondary mirror with a hyperbolic shape that redirects the solar concentration towards the ground receiver. This paper overcomes the main limitation of the previously proposed hyperbolic secondary reflector. A new secondary reflector composed by several fixed flat mirrors located at the same height is proposed. A model to calculate the optimal layout of this novel solar field, as well as the efficiency and concentration, is developed and validated against a Monte-Carlo Ray-Tracing software, obtaining relative errors lower than 15%. Two new dimensionless parameters are proposed to facilitate the design of the flat beam-down linear Fresnel reflector. The concentration, optical efficiency and receiver width can be easily obtained, without performing any simulation, as a function of the dimensionless parameters. This novel solar field can achieve concentration ratios of up to 31 and optical efficiencies of up to 60%, obtaining similar concentrations with better optical efficiency than a field using a hyperbolic reflector.

1. Introduction

A Beam-Down Linear Fresnel Reflector (BDLFR) is a solar concentrating system that provides a solar heat flux on a receiver located at the ground level. BDLFR solar system consists of two reflection stages. First, linear Fresnel reflectors (LFR) aim the solar irradiation to a second stage of mirrors. This second stage beam-downs the solar heat flux towards the receiver, in which heavy materials are thermally processed. This concept was firstly proposed in Ref. [1] combining the advantages of Linear Fresnel technology and point-focus beam-down systems.

On one hand, LFR solar fields employ slightly bended mirrors that concentrate linearly the solar irradiation on a lightweight solar receiver, which is located elevated to avoid blockages and improve the optical efficiency [2,3]. Multiple works have been proposed to improve LFR technology in different ways [4]. Abbas and Martínez-Val studied the influence of mirror width and gap on the performance of the field [5], while Benyakhlef et al. [6] analyzed the effect of the curvature of the mirrors used on the obtained concentration. Mills and Morrison [7] proposed a field with two separate receivers and mirrors alternating between both targets to reduce shading and blocking. Barbón et al. optimized small-scale LFR systems [8,9]. Kincaid et al. [10] proposed a primary field of LFR that floats on a water basin, reducing the installation costs. Zhu et al. [11] studied the behavior of a LFR where the height of the mirrors varies according to their position. Montes et al. [12] analyzed a secondary reflector located in the receiver to improve the performance of the field. However, one of the limitations of LFR solar field is the elevated location of the receiver to properly receive the incoming concentrated solar irradiance. This means that the receiver must be as light as possible to minimize the costs of the supporting structure. To solve this weight problem, Kiyaee et al. [13] and Zhai et al. [14] analyzed the viability of using a Fresnel lens, while Gómez-Hernández et al. [15,16] and Sánchez-González [17] proposed the addition of a secondary beam-down reflector to locate the solar receiver at the ground level.

On the other hand, the secondary beam-down reflector of the BDLFR solar field is based on the point-focus beam-down technology [18], where 3-axis heliostats aim the solar irradiation towards a central reflector that is installed on a beam-down tower. This secondary reflector takes advantage of the optical properties of bifocal geometries, such as ellipsoids or hyperboloids, where the

* Corresponding author.
E-mail address: setaramo@ing.uc3m.es (S. Taramona).

https://doi.org/10.1016/j.renene.2022.01.104

Acronyms

BDF	Beam-down fraction
BDLFR	Beam-down Linear Fresnel Reflector
CPC	Compound Parabolic Concentrator
DSFH	Dimensionless solar field height
DRW	Dimensionless receiver width
LFR	Linear Fresnel reflector
RE	Relative error

Nomenclature

a	Hyperbola main semiaxis [−]
c	Hyperbola linear eccentricity [−]
C	Concentration of flux density [−]
C_g	Geometric concentration ratio [−]
N_r	Number of rows of mirrors on each side of the receiver [−]
w	Width [m]
x	Distance associated with the width of the field [m]
y	Distance associated with the height of the field [m]
α	Auxiliary angle [°]
β	Mirror slope angle [°]
ζ	Loss factor [−]
η	Efficiency [−]
θ_{sun}	Half angle of the solar disk [mrad]

Subscripts

bd	Beam-down
cos	Cosine effect loss
end	End loss factor
f	Higher focus
i	Primary mirror index
int	Intersection point
j	Secondary mirror index
lim	Limiting line
m	Primary mirrors
rec	Receiver
sb	Shadows and blockages
sec	Secondary reflector induced losses
sf	Complete solar field
sp	Spillage at the receiver

sunrays aimed to an upper focal point are redirected towards the lower focal point, which is located on the aperture plane of the ground solar receiver [19,20]. Ideal hyperbolic figures are preferred to define the secondary reflector as lower supporting structures are required [19,21,22]. However, this hyperbolic geometry implies the magnification of the sun image on the solar receiver plane [23], increasing spillage losses on the receiver, and thus, reducing the solar concentration. Some authors solved this issue by adding a tertiary reflection stage based on the Compound Parabolic Concentrator (CPC) geometry. In this line, Diaogo et al. [24] optimized primary heliostats, central reflector and tertiary CPC for point-focus beam-down optics. Kodama also used a CPC to perform water splitting [25–27]. Besides, point-focus beam-down configuration has been employed in many applications, such as coal gasification [28], limestone ($CaCO_3$) calcination processes [29], steam reforming [30], or energy storage [31–33].

BDLFR solar field merges the advantages of both LFR systems, such as the low cost of primary mirrors, and beam-down optics, which can work with heavy materials as the receiver is placed on the ground. Previous works of the authors showed the strength of this solar field for employing particles as heat transfer fluid in fluidized beds [16] or for performing the hydrothermal carbonization of biomass in twin-screw reactors [34]. Sánchez-González and Gómez-Hernández [17], developed the BDLFR solar field considering a hyperbolic cylinder as secondary reflector to concentrate linearly on the ground, where the solar concentration ratio is defined as the product of the ratio between the collector aperture and the receiver width, and the global optical efficiency of the solar field. Despite the high concentration ratios obtained for the optimal configurations (C = 8–40 showing solar efficiencies of 40–70% without using a CPC), the use of a hyperbola-shaped secondary mirror shows some drawbacks. Besides the image magnification issue commented before, the hyperbola eccentricity would produce a significant secondary mirror width, increasing the complexity of the geometry and the shadow losses on the primary field of heliostats. Therefore, this paper proposes the modification of the secondary reflector of the BDLFR solar field described previously in Refs. [16,17], changing from a hyperbolic cylinder to a reflector composed by several flat mirrors located at the same height. Furthermore, this new secondary reflector may reduce the image magnification issue as it is composed by flat mirrors.

In this work, a methodology to design a new secondary reflector composed by flat mirrors at the same height for BDLFR solar fields is presented. The methodology considers the primary LFRs, the new flat secondary reflector and the aperture width of the receiver to optimize the solar field layout. The new flat BDLFR geometry is studied as a function of two newly proposed dimensionless parameters, facilitating the interpretation of results and the design of completely different BDLFR geometries. The methodology employs the edge ray method to simulate the solar beams and their reflection throughout the field. This model is validated against Monte-Carlo Ray-Tracing simulations. The outcome results of the proposed flat BDLFR solar field, which are the solar field geometry, the concentration ratio, the optical efficiency and the receiver width, are compared with the original BDLFR system that employs a hyperbolic cylinder as secondary reflector [17].

2. Flat secondary beam-down reflector

Fig. 1 shows the transversal section of the linear beam-down solar field with a hyperbolic secondary reflector and a new flat secondary reflector. On the left side of Fig. 1, the secondary reflector is described by a hyperbolic cylinder along the Z axis. Sunrays reflected by the Fresnel mirrors towards the higher focal line, are redirected to the lower focal line by the secondary reflector. The lower focus, where the solar receiver is placed, is at the same height as the primary mirror axes. This configuration was previously developed by the authors in Refs. [1,15,17] as a function of the hyperbola eccentricity, which gives an idea of the openness or closeness of the hyperbola.

The proposed flat secondary beam-down reflector is shown on the right side of Fig. 1. The main objectives of the new secondary reflector are:

(i) Install all secondary mirrors at the same height to facilitate the construction of the BDLFR solar field.
(ii) Use flat mirrors to reduce costs.
(iii) Obtain a similar or higher solar field performance comparing the old hyperbolic secondary reflector [1,15,17] and the new flat beam-down layout.

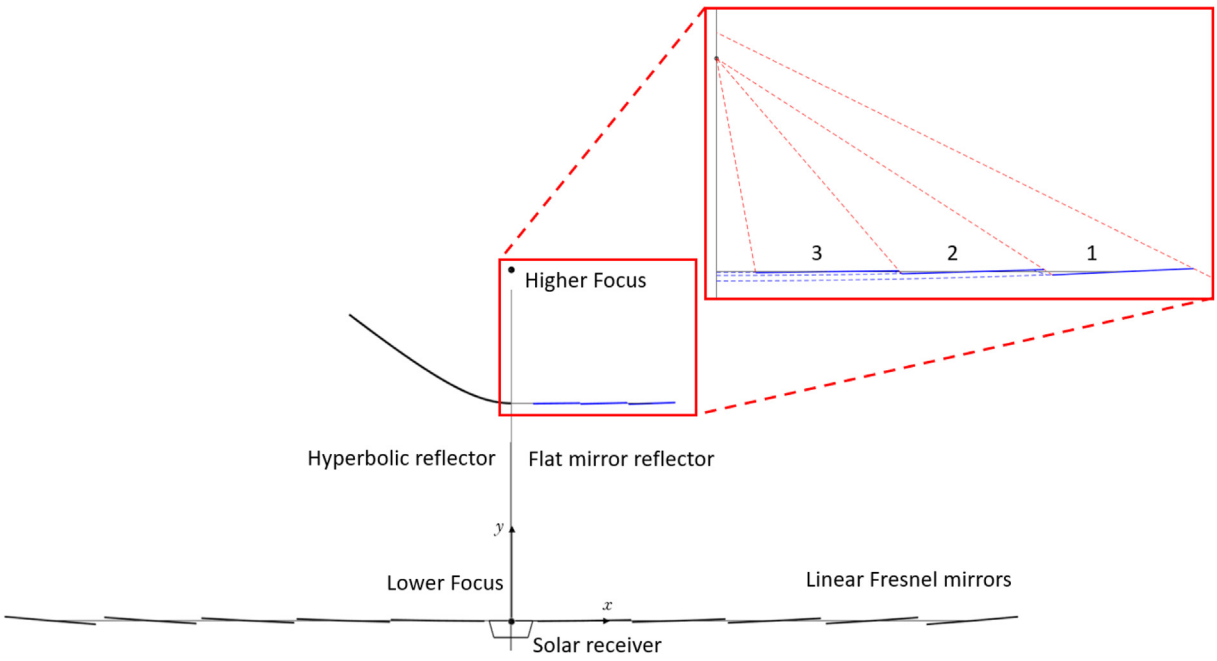

Fig. 1. Linear beam-down solar field. Left X-axis: initial hyperbolic secondary reflector [17]. Right X-axis: new flat secondary reflector.

The first two objectives are achieved by breaking the hyperbolic secondary reflector into multiple flat mirrors that follow different hyperbolas. These hyperbolas have the same higher and lower foci. In this way, the new secondary reflector preserves the interesting optical property of the bifocal figures by which the sunrays reflected by the primary LFR towards the higher focus are redirected towards the lower focus. Furthermore, the flat secondary mirrors are tangent to the hyperbolas, as shown in Fig. 2 for a flat secondary reflector composed by 4 flat mirrors. The calculation of the mirror characteristics, i.e. center position, width and inclination, is explained in the next section. The achievement of the third objective is demonstrated in section 4.4.

In this study a North - South orientation is considered, as this configuration performs better than East - West orientations for LFR solar fields [35]. With the selected orientation BDLFR solar fields have the additional benefit of presenting symmetry along the longitudinal axis, simplifying the design process of the field layout.

3. Methodology

This section describes the procedure used to design the solar field layout equipped with the new flat secondary reflector. The model inputs are two dimensionless parameters, the number of primary mirrors and their constant width and an initial null value for the receiver width, while the model outputs are the solar field layout, including the optimal receiver width, the mean solar flux concentration on the receiver and optical efficiency of the solar field. The design conditions for the model are a latitude of 40° North, spring equinox (March 21st) at solar noon.

Since the proposed solar field is symmetric along the longitudinal axis, the model designs and evaluates half of the solar field and then doubles the obtained concentration to obtain the result for the complete field. Additionally, as the proposed field is linear with a North - South orientation, the design process can be done in a bidimensional plane perpendicular to the orientation of the field.

Regarding the solar simulations, edge ray method is used to design the solar field and calculate the solar concentration and optic efficiency. This method assumes that around 95% of the solar radiation is contained within the half angle subtended by the solar disk ($\theta_{sun} = 4.69\ mrad$) [17,19,36]. This energy distribution applies to reflected beams in both primary and secondary mirrors neglecting mirror slope and tracking errors. In this way, the edge rays traced from each mirror would define the solar receiver width.

3.1. Dimensionless parameters

Two dimensionless variables are proposed to present the results of completely different BDLFRs:

- Dimensionless Solar Field Height (DSFH): this parameter relates the higher focus height (y_f) with half of the solar field width, which is calculated as the product of the primary mirror width (w_m) and the number of primary mirrors on each side of the field (N_r). The separation distance between adjacent mirrors is neglected in this dimensionless parameter to simplify the calculations. DSFH is defined as:

$$\mathrm{DSFH} = \frac{y_f}{N_r \cdot w_m} \tag{1}$$

- Beam-down Fraction (BDF): this parameter determines the relative height between the beam-down reflector (y_{bd}) and the higher focus (y_f). It is defined as:

$$\mathrm{BDF} = \frac{y_{bd}}{y_f} \tag{2}$$

The geometrical relations used in the dimensionless parameters can also be represented as a triangle for an easier understanding of the configuration of the solar field, as presented in Fig. 3. The introduction of these two dimensionless parameters allows the definition of the complete geometry of the solar field. For instance, selecting both dimensionless variables and two geometrical parameters, such as the number of mirrors and their width, would define the focal and the secondary reflector height.

Fig. 4 shows the influence of both DSFH and BDF dimensionless

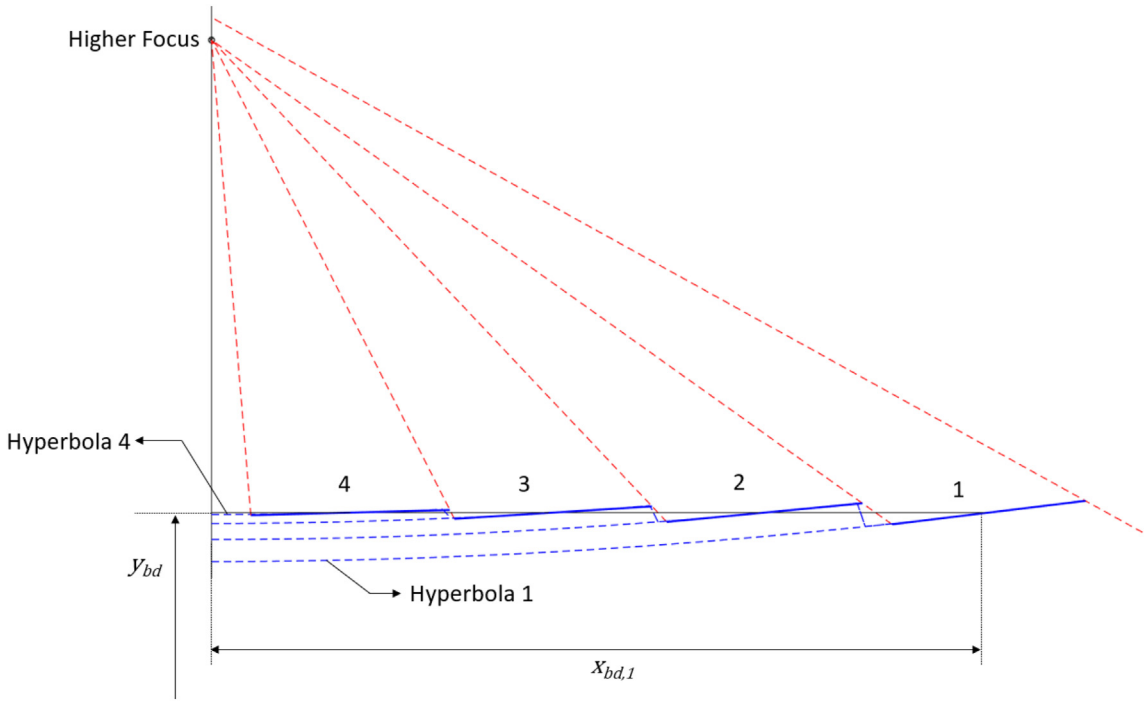

Fig. 2. Flat secondary mirrors with their required position and slope to follow their own hyperbola.

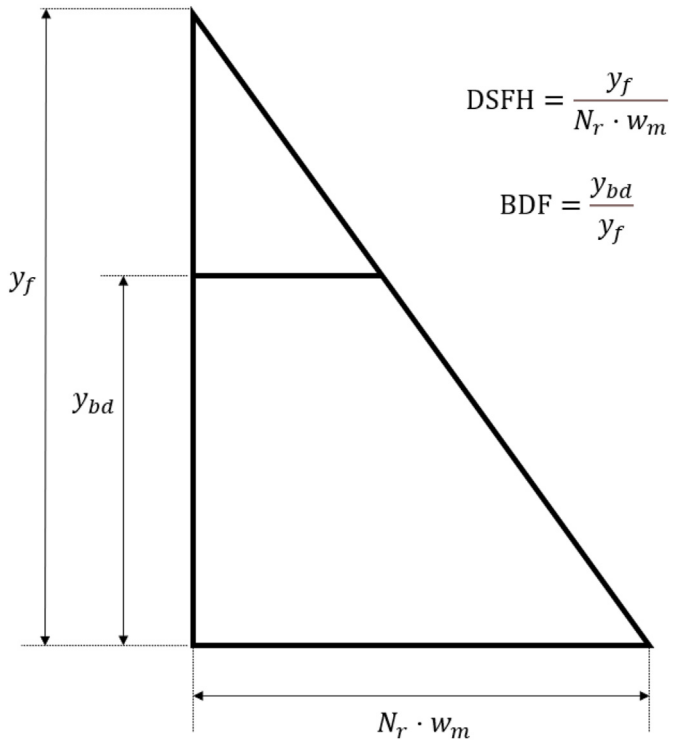

Fig. 3. Geometrical relations of the solar field with the dimensionless parameters.

parameters on the layout of the solar field using the triangular representation. Regarding the solar field height, DSFH < 1 describes wide solar fields showing lower height than total width (Fig. 4-a). A value of DSFH = 1 defines solar fields represented by an isosceles right triangle, showing the same height and total width (Fig. 4-b), while DSFH > 1 represents slim solar fields with higher focal height than total width (Fig. 4-c). Model simulations consider DSFH values between 0.6 and 2.5. On the one hand, DSFH < 0.6 values are neglected as these solar fields would present low focal height, increasing the LFR cosine losses, total secondary reflector width, and the distance between mirrors would become a significant parameter. On the other hand, DSFH > 2.5 shows a high focal height, which increases the receiver width, and thus, reduces the solar concentration.

Regarding the beam-down fraction, BDF, this parameter is associated to the vertical position of the flat secondary mirrors and the hyperbola eccentricity. BDF can range between 0.5 and 1. The lowest constraint is limited by the eccentricity of the hyperbola associated to each flat mirror. As shown in the previous section, each flat mirror is related to a hyperbola that is constrained by the position of the higher and lower foci. For BDF <0.5, the geometrical constraints prevent a hyperbola to be defined [17]. BDF = 0.5 would create a wide secondary reflector with high shadow losses on the primary reflectors. Besides, such a value means that the secondary reflector would be composed by flat mirrors installed horizontally since all associated hyperbolas would be flat, increasing the image magnification on the ground [23]. BDF = 1 would produce a secondary reflector located at the higher focus and defined by a hyperbola with infinite curvature. Therefore, the following sections consider BDF values ranging from 0.51 to 0.8. To clarify the BDF influence on the solar field geometry, Fig. 4 shows the position of the flat secondary reflector for the defined BDF limits.

3.2. Primary mirrors

To properly define the primary mirror field Mathur's Method [37] is used alongside Snell's reflection law. This procedure defines the correct position for every mirror, avoiding the blocking of the reflected sun rays for solar noon conditions. Knowing the desired mirror's width, the higher focus position and estimating the receiver's width, this method determines both the position and the slope for each mirror through different iterations to avoid said

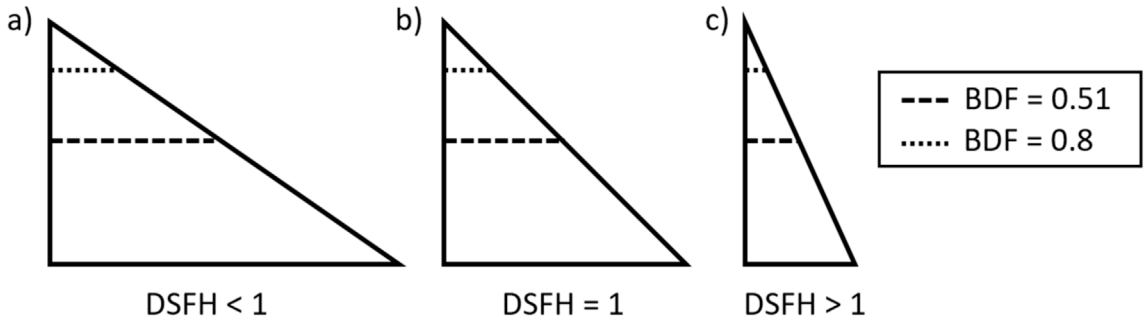

Fig. 4. Solar field configurations as a function of DSFH and BDF: (a) DSFH < 1, (b) DSFH = 1, (c) DSFH > 1.

blockages. However, to apply this method the position of the first LFR row has to be defined before calculating the rest of mirror rows. The position of the center of this first mirror is defined as the sum of half the receiver width and a half and a twentieth of the mirror width ($\frac{w_{rec}}{2}+\frac{w_m}{2}+\frac{w_m}{20}$), where the last parameter is incorporated to take into account the mirror's thickness, so it can freely rotate without colliding with the receiver. Additionally, these primary mirrors present a slight curvature of radius equal to twice the distance to the higher focus [2]. Incorporating this curvature definition to Mathur's Method, the three required parameters can be calculated for each mirror using multiple iterations.

3.3. Beam-down mirrors

The secondary reflector is composed by several fixed flat mirrors that are located elevated above the primary Fresnel reflectors. The position of the furthest primary mirror ($x_{m,Nr}$), the height of the higher focus target (y_f), and the height at which the secondary reflector is located (y_{bd}) are needed to calculate the number, width (w_{bd}), position ($x_{bd,j}$) and inclination (β_j) of the flat secondary mirrors.

The first parameter to define is the width of the secondary mirrors. This width is calculated considering edge rays traced from the last mirror row aimed towards the higher focus, as shown in Fig. 5. To simplify the calculations, all flat secondary reflectors have the same width.

After obtaining the beam-down mirror width, the remaining parameters must be calculated considering the following restrictions:

- Every mirror must be associated to a hyperbola, and every hyperbola has the same focal distance to ensure that all rays are redirected towards the solar receiver.
- Each flat secondary mirror is tangent to the associated hyperbola at the beam-down height, this allows the flat mirrors to retain part of the interesting optical properties of the hyperbola, where all the rays pointed towards the higher focus are redirected towards the lower one.
- All secondary mirrors must be located at the design beam-down height.
- The position of each secondary mirror is such that its furthest edge is either defined by the solar cone, similar to the calculation of w_{bd}, or by the closest edge of the next secondary mirror. Fig. 5 identifies both cases as “limiting line”. This step prevents blockings between secondary mirrors, as well as losses between mirrors.

These assumptions are translated to the equation system shown in Eqs. (3)–(7) to calculate the center position of each beam-down mirror ($x_{bd,j}$), its slope (β_j), its furthest edge ($x_{int,j}$ and $y_{int,j}$) and the main semiaxis of the associated hyperbola (a_j):

$$y_{int,j} = y_{lim,j} - \left(\tan\left(\alpha_{lim,j}\right)\cdot\left(x_{int,j} - x_{lim,j}\right)\right) \tag{3}$$

$$y_{int,j} = y_{bd} + \left(\tan\left(\beta_j\right)\cdot\left(x_{int,j} - x_{bd,j}\right)\right) \tag{4}$$

$$\frac{w_{bd}}{2} = \left|\sqrt{\left(y_{int,j} - y_{bd}\right)^2 + \left(x_{int,j} - x_{bd,j}\right)^2}\right| \tag{5}$$

$$y_{bd} = c + \sqrt{a_j^2 + \left(\frac{a_j \cdot x_{bd}}{\sqrt{c^2 - a_j^2}}\right)^2} \tag{6}$$

$$\tan\left(\beta_j\right) = \frac{a_j^2 \cdot x_{bd,j}}{\left(c^2 - a_j^2\right)\sqrt{\frac{a_j^2 \cdot x_{bd,j}^2}{\left(c^2 - a_j^2\right)} + a_j^2}} \tag{7}$$

where the input parameters are: the secondary mirrors width w_{bd}, the beam-down height y_{bd}, the linear eccentricity of the hyperbola defined as $c = y_f/2$, and the coordinates (x_{lim}, y_{lim}) and angle (α_{lim}) of the limiting line that defines the edge of the secondary reflector as shown in Fig. 5. The limiting line is calculated using either the reflection of the solar cone from the last primary LFR row, or the coordinates of the edge of the next furthest secondary mirror and the angle of the line that connects this point with the higher focus. Note that the position of each secondary mirror depends on its inclination angle and its edges, and thus, the mirror center may not be the same as the position of the reflected sunray at beam-down height.

This equation system is solved iteratively starting from the furthest mirror of the solar field and proceeding towards the center of the field until there is not enough space to introduce an additional beam-down mirror with the desired width. After that, the receiver width is computed.

3.4. Solar receiver width

The solar receiver width is calculated considering the reflection of the subtended cone of solar radiation from the center of the LFR, as was previously done in Ref. [17]. The width of the receiver aperture is set applying the edge ray method to all primary mirrors and keeping the maximum value. This value is compared to the initial solar receiver width. The convergence of the method is obtained when the new solar receiver width contains all the rays reflected from the primary field, as shown in Fig. 6. Furthermore, as

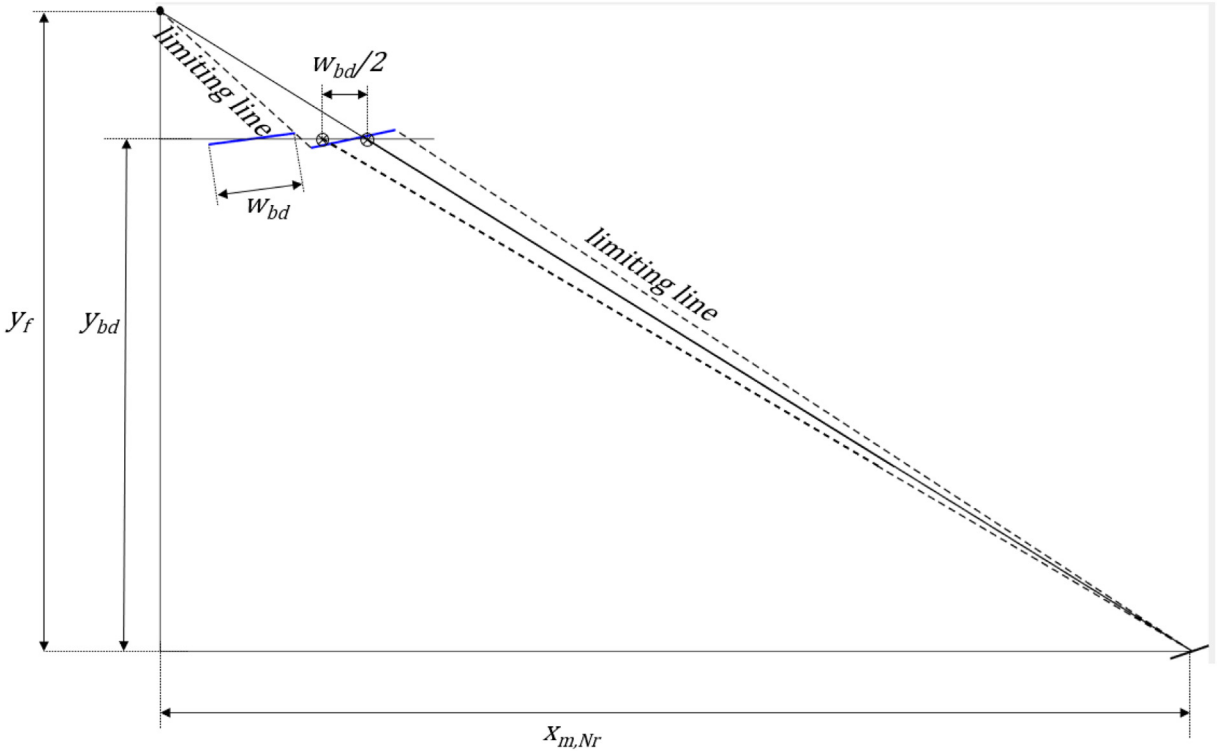

Fig. 5. Calculation of the secondary mirror width.

the edge ray method has low computing costs, this method is initialized assuming a negligible solar receiver width ($w_{rec} = 0$) to do at least 2 iterations to compute the solar field design. This allows to obtain the optimal receiver width, defined as the minimum width that gathers all the simulated sunrays.

The dimensionless receiver width (DRW) is defined as shown in Eq. (8) to make easier the interpretation of the results.

$$\mathrm{DRW} = \frac{w_{rec}}{w_m \cdot N_r} \tag{8}$$

Once this procedure is finished, the solar field is designed as shown in Fig. 6. In the presented example the number of Fresnel rows on each side of the field is $N_r = 15$, with a mirror width of $w_m = 0.5$ m, a focal height of $y_f = 9.75$ m and a beam-down height of $y_{bd} = 7.3125$ m, which means DSFH = 1.3 and BDF = 0.75 which allows a concentration of $C_{sf} = 15.54$ with an efficiency of $\eta_{sf} = 51.25\%$ using the procedure explained in the following sections. As it can be seen the primary mirrors are located near the ground, where no shading or blockages occur between them at noon, the beam-down is located at the desired height and

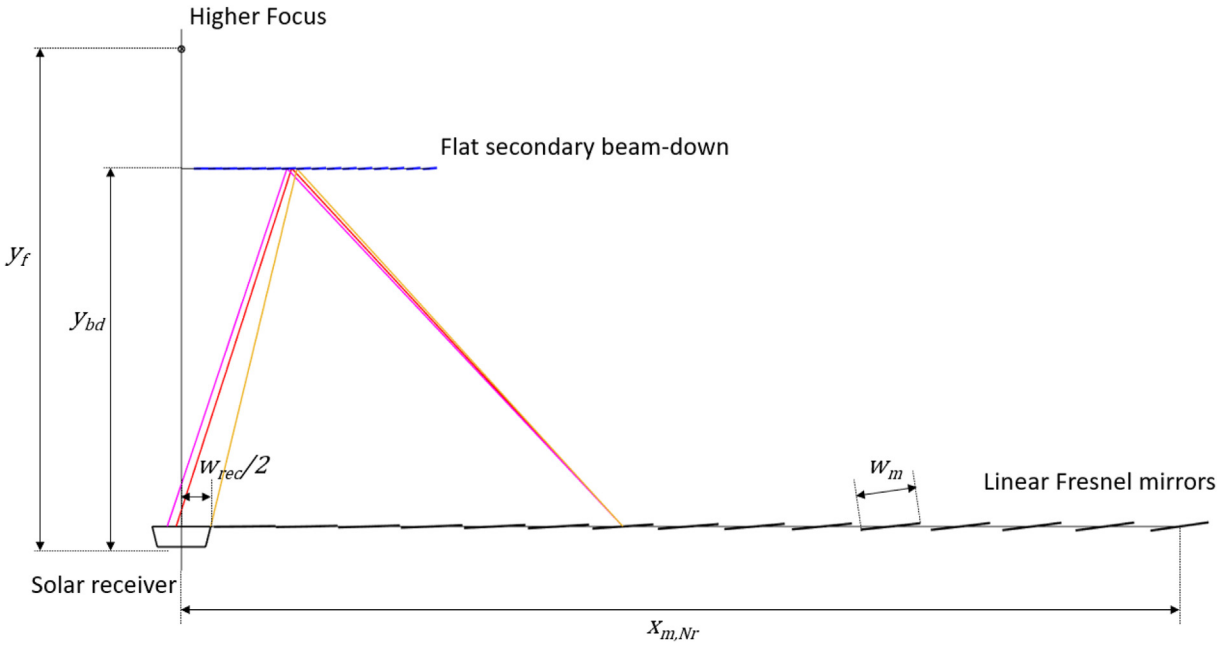

Fig. 6. Complete flat BDLFR solar field.

composed by several flat mirrors, and the solar flux concentration reaches the receiver aperture.

3.5. Solar concentration and optical efficiency

As pointed in Ref. [17], the overall optical efficiency of the BDLFR solar field represents the fraction of irradiance that reaches the solar receiver and the maximum potential irradiance that could reach the primary field, and it can be expressed as the average of each mirror efficiency, Eq. (9):

$$\eta_{sf} = \frac{1}{N_r} \cdot \sum_{i=1}^{N_r} \eta_{m,i} \tag{9}$$

where $\eta_{m,i}$ is the optical efficiency of each primary mirror. Such efficiency is the product of all optical losses that can take place in the BDLFR solar field:

$$\eta_{m,i} = \eta_{cos,LFR,i} \cdot \eta_{cos,sec,i} \cdot \rho_{LFR} \cdot \rho_{sec} \cdot \zeta_{sb,LFR,i} \cdot \zeta_{sb,sec,i} \cdot \zeta_{end} \cdot \zeta_{sp,i} \tag{10}$$

Once the solar field is completely designed, the next step is to define the optical efficiency and the incident mean flux concentration. This process is similar to the one described in Ref. [17] with some additional modifications to adjust to the proposed changes.

- Primary mirror cosine factor ($\eta_{cos,LFR}$): this factor defines the reduction of solar collection area due to the inclination angle between the solar irradiation and the reflected beams. For the primary mirrors, it is defined as the cosine of the angle between the vector normal to each mirror, and the vector of the incident central sun ray. This factor is calculated in a three-dimensional to consider the latitude and the day of the year.
- Secondary cosine factor ($\eta_{cos,sec}$): in a similar way to the primary mirrors, there are also cosine losses in the flat beam-down mirrors. In this case, this efficiency is calculated as the cosine of the angle between the incident rays from each primary mirror and the beam-down mirror normal.
- Reflectivity (ρ): proportion of direct irradiation reflected by the mirrors. It considers the inherent properties of the mirror, as well as how clean it is. In this study, this loss factor is neglected ($\rho_{LFR} = 1$ and $\rho_{sec} = 1$) to simplify the extrapolation of results.
- LFR shading and blocking ($\zeta_{sb,LFR}$): fraction of direct and reflected irradiance that gets blocked by adjacent primary mirrors. As the positions of these mirrors have been determined using Mathur's Method, this factor is negligible for design conditions.
- Beam-down shading ($\zeta_{sb,sec}$): the surface of primary mirrors that does not receive direct solar irradiance because it is directly under the secondary reflector has a null efficiency. The value of this parameter is calculated proportionally to the exposed primary LFR width for each mirror. This factor is highly influenced by the geometry of the solar field and can be studied with the previously presented dimensionless parameters. For a constant number of mirrors with a fixed width, an increase of BDF reduces the total secondary width, diminishing the shading.
- End factor (ζ_{end}): considers the reflected irradiance lost in the longitudinal axis of the field. This factor is highly dependent on the solar altitude. With a proper longitudinal design, or considering a long enough solar field, this factor is negligible.
- Spillage (ζ_{sp}): fraction of the irradiance finally intercepted at the solar receiver. The methodology ensures that all reflected beams fall within the limits of the receiver, so this loss factor can be neglected.

Therefore, at the equinox noon design conditions, the optical performance is simplified to:

$$\eta_{m,i} = \eta_{cos,LFR,i} \cdot \eta_{cos,sec,i} \cdot \zeta_{sb,sec,i} \tag{11}$$

The mean concentration ratio of flux density of each mirror ($C_{m,i}$) can be calculated using the geometric concentration ratio (C_g) and its optic efficiency ($\eta_{m,i}$), which are mathematically expressed in Eqs. (12) and (13).

$$C_g = \frac{2 \cdot N_r \cdot w_m}{w_{rec}} \tag{12}$$

$$C_{m,i} = C_g \cdot \eta_{m,i} \tag{13}$$

Finally, the mean concentration ratio of flux density of the solar field is calculated considering the symmetry of the solar filed:

$$C_{sf} = 2 \cdot \sum_{i=1}^{N_r} C_{m,i} \tag{14}$$

The complete design process can be reviewed in Fig. 7. Once the input parameters are defined, the model uses equations (1) and (2) (step 1 in Fig. 7) to obtain the remaining physical parameters: the focal and beam-down height. After obtaining the required dimensions, the disposition of the primary mirrors is calculated using Mathur's Method (2), allowing to obtain the optimal position, slope and curvature of each primary mirror for the current design conditions. Once the primary field layout is calculated, the width for the beam-down flat mirrors is calculated using the solar aperture from the reflection of the mirror located furthest away from the receiver (3). With this new dimension, the position and slope for all the mirrors that compose the secondary reflector can be calculated (4). After obtaining the complete layout of the solar field, a simulation of the sunrays (considering the solar aperture) reflected by each primary mirror towards the beam-down, and the posterior reflection towards the receiver area is performed, obtaining the optimal receiver width for the current solar field layout (5). This optimal width is compared with the initial value (6), and if the receiver is not wide enough, steps 2–6 are repeated with the updated receiver width. If it is wide enough the final outputs of the model are calculated, which are the optical efficiency, the final receiver width, and the concentration.

4. Results

Once the model is developed in MATLAB, the results are validated using a Monte-Carlo Ray-Tracing software. For this task, SolTrace tool developed by NREL [38] has been used to compute the mean concentration ratio. Then, the model performance is studied comparing different solar field geometries. Finally, the flat secondary reflector proposed in this work is compared with the hyperbola-shaped secondary reflector initially developed in Refs. [15,17].

Different design charts are obtained using the model and the SolTrace results. These charts allow to determine the performance of the designed solar field from the dimensionless parameters, this means, knowing the relative geometry of the solar field. Knowing the solar field width and the focal and beam-down height, the concentration, efficiency and receiver width can be obtained using the presented charts, without requiring a re-evaluation with the proposed model.

4.1. Solar field concentration and validation with Monte-Carlo Ray-Tracing

Fig. 8 compares the average concentration ratio obtained using

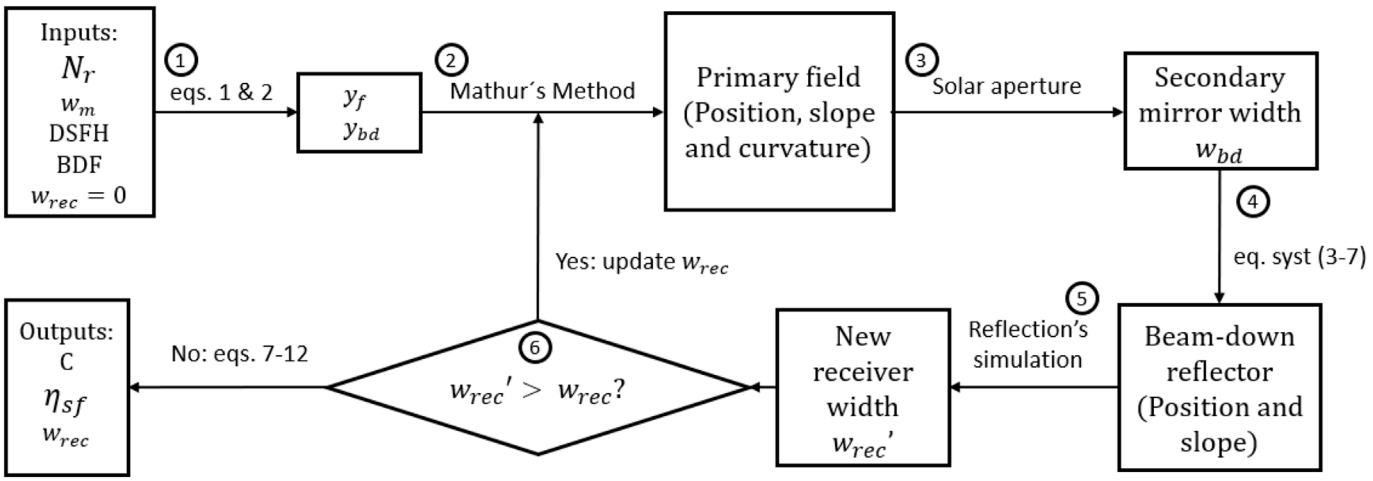

Fig. 7. Flowchart representing the procedure to obtain the concentration and efficiency.

the proposed model (solid line) and SolTrace (dotted line) for the DSFH and the BDF ranges defined before, for example, having DSFH = 1.25 and BDF = 0.65 results in a concentration of approximately 26 suns. As it can be seen, similar trends are obtained by both methods. Low concentrations are obtained when DSFH values approach the established limits. On one hand, low DSFH values mean wider solar fields, having a lower focal point means that the space between mirrors increases to avoid shadows and blockages, which reduces the optical efficiency of the field due to cosine factor of the primary mirrors.

On the other hand, increasing the focal point height (higher DSFH values) results in wider solar receivers (as seen in Fig. 11) and a higher fraction of shaded primary mirrors, which lowers the obtainable concentration.

Fig. 9 shows the relative error (RE) between SolTrace simulations and the model results, where positive values indicate an overestimation of the concentration ratio by the model. Overall, the model deviates from SolTrace results between 15% and −10% for all DSFH and BDF values.

4.2. Optical efficiency and receiver width

This subsection illustrates the optical efficiency of the flat DSFH solar field (Fig. 10) and the dimensionless receiver width (Fig. 11). The optical efficiency increases with high DSFH and BDF values. This result is explained by the shadow losses, which are minimized when the beam-down is located at great height (BDF ~ 0.8) decreasing the total width of the secondary reflector without increasing the percentage of LFR mirrors under the casted shadow. Taking the same pair of parameters as the concentration example (DSFH = 1.25 and BDF = 0.65), all solar fields with these dimensionless values have an optical efficiency close to 47.5%.

Note that the designs with the highest concentration (DSFH = 1.25 and BDF = 0.55) show low optical efficiency. This is a consequence of the low BDF value, which ensures a wide secondary reflector, and therefore, higher shading losses.

In traditional LFRs, such as the one studied in Ref. [2], the optical efficiency is around 65%. Comparing with the efficiency range obtained with the proposed design the effect of the secondary reflector can be observed, where the highest optical efficiency of

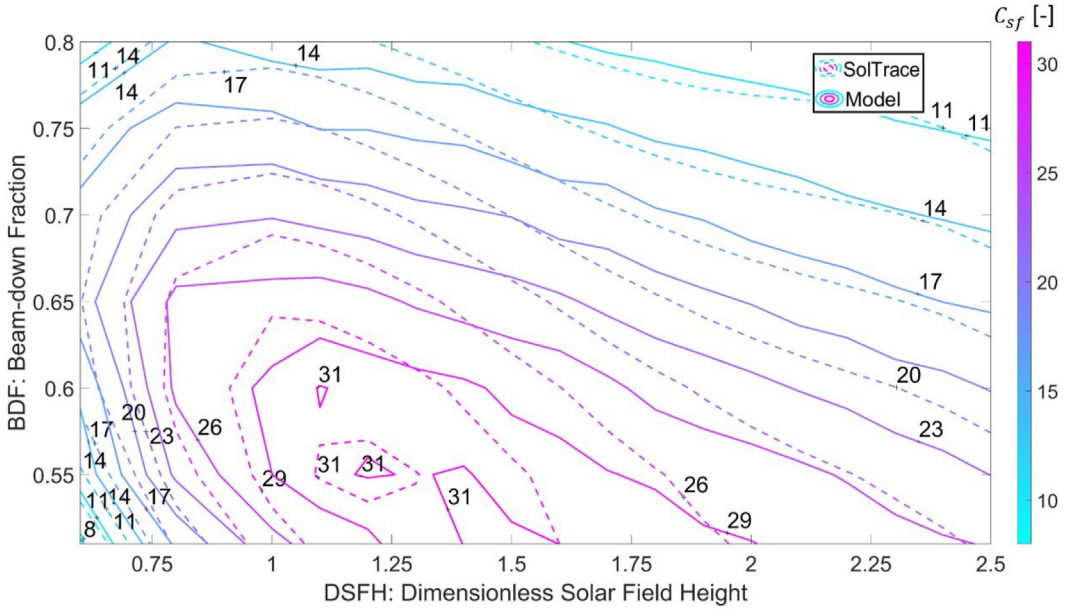

Fig. 8. SolTrace (dotted line) and model (solid line) concentration at the receiver aperture.

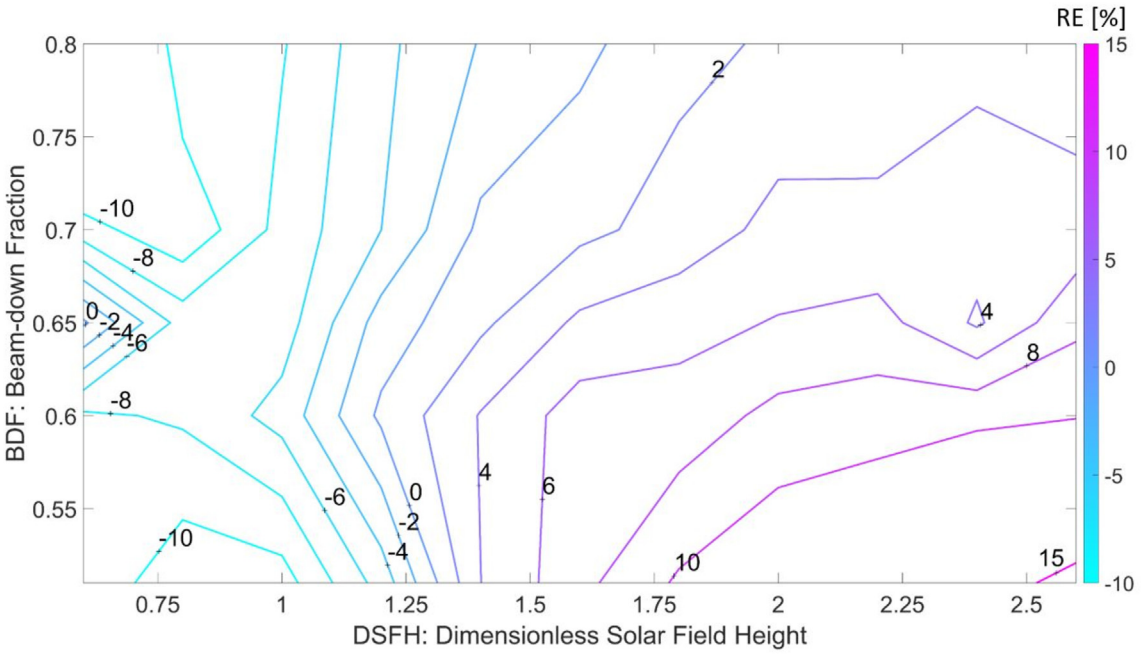

Fig. 9. Relative error of the concentration values between SolTrace and the proposed model.

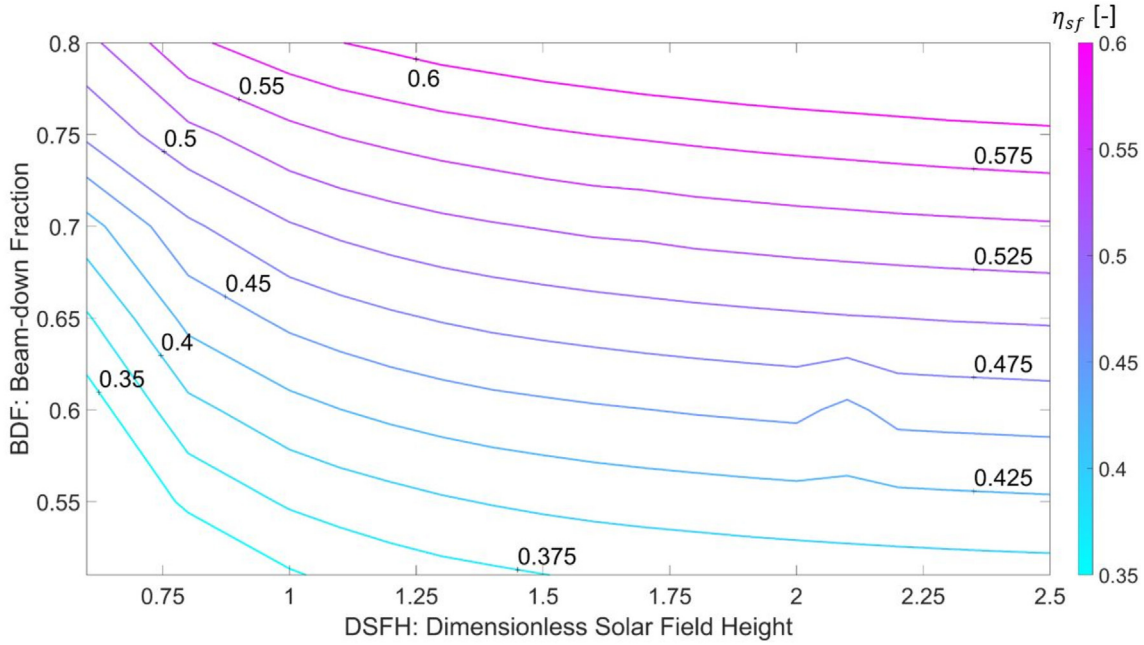

Fig. 10. Flat BDLFR optical efficiency.

around 60% can be achieved when the beam-down shading is low, an eficciency of a similar order of magnitude as the one obtained with traditional LFRs. This result is fairly promising considering the range of possibilities that this new proposed design opens up.

Fig. 11 shows the dimensionless receiver aperture. This dimensionless parameter is the last result obtained in the model, as explained before. The minimum aperture is obtained for DSFH = 1.25 and BDF = 0.55, which showed the maximum concentration in Fig. 8. This is explained by the low sunrays dispersion generated by the beam-down for such DSFH and BDF values. A high BDF value means that the reflector would be located at a higher altitude, increasing the magnification; the same happens with high DSFH values. On the other hand, if DSFH is too low, a high number of primary mirrors would be shaded, and the sunrays that define the receiver aperture would come from a further distance, increasing the image magnification.

To finish the example started with the concentration chart, with the presented set of dimensionless values (DSFH = 1.25 and

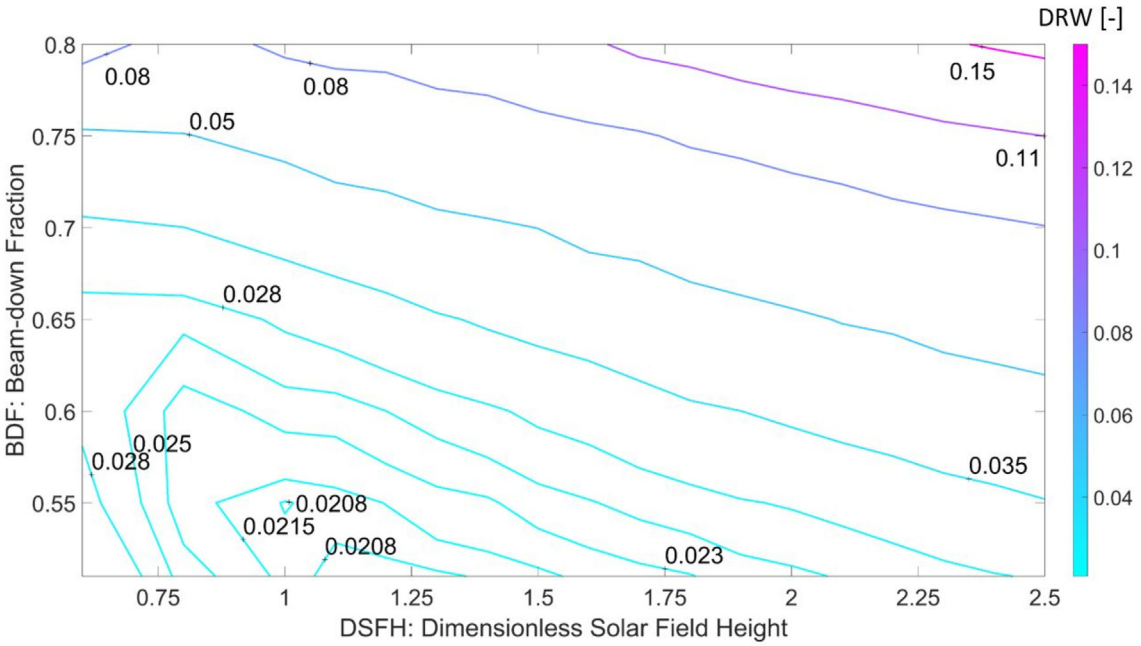

Fig. 11. Dimensionless receiver width.

BDF = 0.65), the dimensionless receiver width is close to 0.033. This means that to obtain the required receiver width, this result obtained from the charts must be multiplied by half the solar field width, so a wider solar field means a wider receiver.

An in-depth explanation of the usage of the presented design charts is presented in the following section and in Appendix B.

4.3. Design charts usage

In this section, two properties for the design charts are presented. The first one is the consistency of the results for different solar fields with the same dimensionless parameters, while the second one is the usefulness of the charts themselves for different circumstances.

Regarding the first property, to demonstrate the consistency of the proposed design two different points in the diagram are be studied, case A has a DSFH = 1.25 and a BDF = 0.65, and case B has a DSFH = 1.75 and a BDF = 0.7. As each point on the diagram allows infinite solar field designs, three solar field layouts are defined for this case study. The first field is composed of 15 LFR mirrors 0.5 m wide on each side of the receiver, the second one has 40 rows 0.1 m wide, and the third field has 10 rows 0.2 m wide. All the studied combinations are compiled in Table 1, and the difference between case A and B is represented in Fig. 12.

The model results are displayed in Table 2. Additionally, the design charts for the studied cases are shown in Appendix A. As expected, the concentration, solar field efficiency and dimensionless receiver are the same for all of the studied solar field layouts for cases A and B. As it can be seen, both the receiver aperture and the beam-down height decrease with the total LFR width, being field number 1 the widest.

The first convenience of the charts is that, for a known couple of dimensionless parameters the performance of the solar field can be easily determined with a simple examination of the charts. This demonstrates the core usefulness of the presented charts: being able to obtain results without simulations.

Table 1
Studied cases.

Configuration	DSFH [−]	BDF [−]	N_r [−]	w_m [m]
A1	1.25	0.65	15	0.5
A2			40	0.1
A3			10	0.2
B1	1.75	0.7	15	0.5
B2			40	0.1
B3			10	0.2

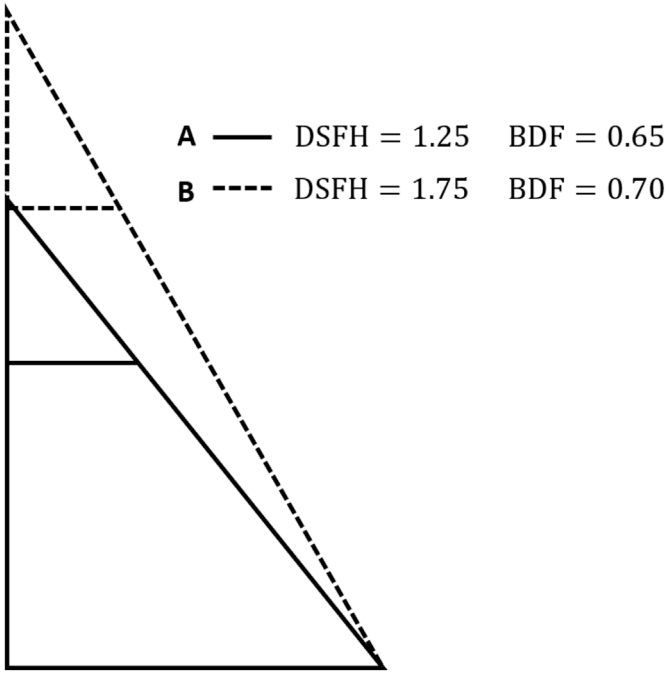

Fig. 12. Dimensionless triangle configuration of cases A and B.

Table 2
Model results for various solar fields with constant dimensionless parameters.

Configuration	N_r [−]	w_m [m]	C_{sf} [−]	η_{sf} [%]	DRW [−]	y_f [m]	y_{bd} [m]	w_{rec} [m]
A1	15	0.5	26.4	47.7	0.033	9.38	6.09	0.24
A2	40	0.1				5.00	3.25	0.13
A3	10	0.2				2.50	1.63	0.07
B1	15	0.5	17.7	53.6	0.058	13.13	9.19	0.44
B2	40	0.1				7.00	4.90	0.23
B3	10	0.2				3.50	2.45	0.12

Going beyond this first layer and delving deeper in the dimensionless parameters, these charts allow to consider both requirements and restrictions for the layout design. For example, for a specific number of mirrors with a determined width, both the concentration and DRW can be determined to supply the required heat for an industrial process. Other restrictions can also be considered, such as the available space for the solar field, or the mirror. An example with these considerations is developed in Appendix B.

Another interesting comparison is the behavior of different configurations through the day. In Fig. 13 the evolution of the concentration for three different days is represented: for the summer and winter solstice, and for the equinoxes.

It can be seen how for design conditions the concentrations have similar values for the three presented days, while for the rest of the day the case with the higher number of mirrors (A2) produces the highest concentration. This difference happens because of the higher shading produced by wider primary mirrors for the hours outside the design condition. A more precise design could be achieved taking into account the offset hours, the yearly energy annual production, the environmental costs and the application process.

4.4. Benefits of a flat beam-down

Finally, the new flat BDLFR is compared with a hyperbolic secondary reflector. The methodology described in Ref. [17] is used to design the hyperbola and its associated primary LFRs. The same input parameters have been employed: number of LFR mirrors with their respective width, and higher focus height. Furthermore, the vertex of the hyperbola is located at the same height of the flat beam-down, in the same way as displayed in Fig. 1. The comparison results are summarized in Table 3.

For the flat secondary reflector, both the model and the SolTrace concentrations are presented, while the concentration for the hyperbolic beam-down is obtained only using SolTrace. As shown in Table 3, the first interesting result is that the concentration consistency for a set of dimensionless parameters found in the flat beam-down, is not obtained when employing a hyperbolic secondary reflector. When simulating the solar field with a hyperbolic beam-down the number of mirror rows, focal height and hyperbola eccentricity play a key role in the obtainable concentration of the solar field [17]. Therefore, the concentrations greatly differ and can be higher or lower than the concentration obtained using flat mirrors for the beam-down.

The solar field efficiency is always higher for the flat beam-down reflector for all studied cases. This is because the flat mirrors composing the secondary reflector have an overall better performance than the curved mirror. Particularly when considering the solar aperture, flat mirrors do not induce as much magnification as the hyperbolic cylinder.

Case B3 is used to compare the efficiency of the flat and hyperbolic beam-downs. The receiver width (w_{rec}) is similar for both reflectors while the higher focal point stays fixed, which means that the primary mirrors would be located in similar positions, and therefore, the associated cosine factor is similar in both cases. Comparable shading losses are also expected, as the total width for the flat secondary reflector is 1.255 m, while the hyperbolic reflector is 1.252 m. This similarity in shading and primary mirror positions means that the variation of the efficiency is highly affected by the shape of the beam-down.

The consistency obtained for the novel BDLFR allows an easier

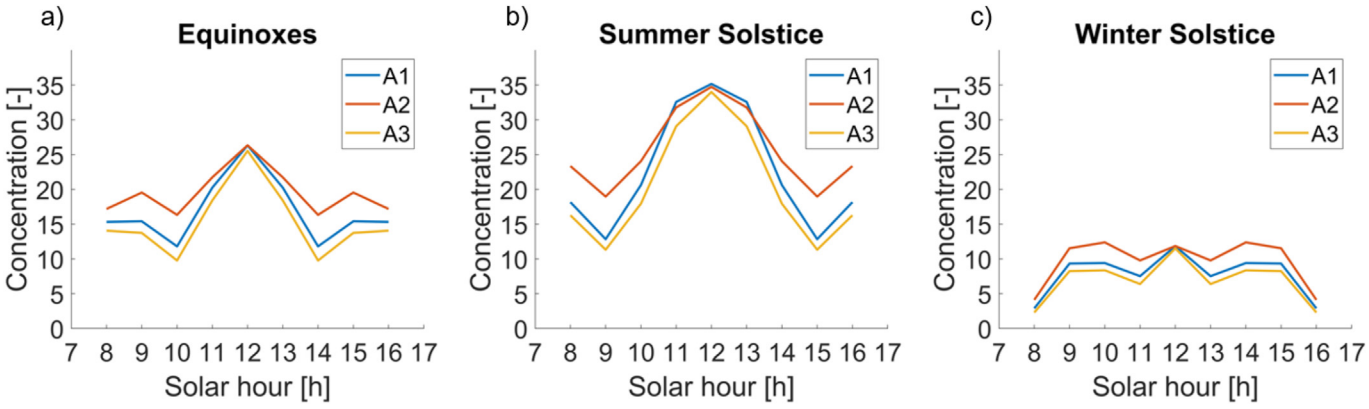

Fig. 13. Concentration through the day for case A. a) March 21st and September 21st, b) June 21st and c) December 21st.

Table 3
Comparison of flat and hyperbolic BDLFR.

	Flat B-D				Hyperbolic B-D		
	$C_{sf,model}$ [−]	η_{sf} [%]	$C_{sf,SolTrace}$ [−]	w_{rec} [m]	$C_{sf,SolTrace}$ [−]	η_{sf} [%]	w_{rec} [m]
A1	26.4	47.7	26.0	0.24	25.5	44.7	0.26
A2				0.13	27.7	43.4	0.13
A3				0.07	23.8	44.5	0.08
B1	17.7	53.6	17.1	0.44	14.1	33.8	0.36
B2				0.23	20.2	45.7	0.18
B3				0.12	19.1	47.4	0.10

optimization of the performance and layout of the solar field, with all the variables reduced in 2 parameters, the best available combination is easy to identify.

Traditional LFRs, with no secondary reflectors, can achieve concentrations between 30 and 80 suns [39], while the highest obtainable concentration with the proposed design is 31 suns. This drawback was expected, since adding a secondary reflector that casts shading on some primary mirrors and reduces the optical efficiency of the field impacts the obtainable concentration. However, when considering both, the possibilities that open up when including the beam-down, and the maximum obtainable concentration that is within the lower end of the traditional LFR concentration range, this proposed BDLFR technology is suitable as a viable solution for supplying solar energy to process heavy materials.

Analyzing the economic implication of the different beam-down reflectors, the costs of flat and curved mirrors can be estimated as 72 €/m^2 and 132.23 €/m^2 respectively, using the data available in Refs. [40,41]. Considering again the case B3, the sum of all the required mirror widths for the flat reflector is 1.178 m while the curve length of the hyperbolic reflector is 1.245 m, combining these values results in a saving of 79.81 € for each meter of the solar field. Therefore, the manufacture of a hyperbola-shaped secondary reflector increases the specific cost around 80% compared to a flat-shaped reflector [40,41].

5. Conclusions

A novel solar field that couples a traditional Fresnel collector and a flat beam-down reflector has been proposed in this paper, alongside a model that calculates the layout of this new kind of field, as well as the efficiency and the concentration. This novel solar field meets the required objectives: the beam-down reflector is constructed with fixed flat mirrors located at the same height, and this design allows a better performance than using a hyperbolic reflector.

Three design charts have been developed for this novel solar field. These charts allow to easily design the desired solar field to meet the desired outputs, where the only required inputs are the proposed dimensionless parameters: the Dimensionless Solar Field Height (DSFH) and the Beam-down Fraction (BDF). In this way, for the design conditions (a latitude of 40° N and midday conditions for spring equinox), using both dimensionless parameters the optical efficiency, the concentration of the solar field, and the optimal receiver width can be easily obtained just by looking at the charts.

The maximum obtainable concentration of the proposed solar field is around 31 suns for values of DSFH ~1.24 and BDF ~0.55, with an optical efficiency of η_{sf} ~39% and a dimensionless receiver width of DRW ~0.021. The minimum receiver width is approximately 0.0208 obtained for values of DSFH from 1.1 to 1.26 and low BDF values. The maximum efficiency is higher than 60% and is obtained for BDF >0.75 and DSFH > 1.25. The maximum relative error between the developed MATLAB model and the validation with SolTrace remains lower than 15% for all studied cases.

The new flat BDLFR overcomes the main disadvantage of the previously proposed hyperbolic reflector, which was the manufacturing challenge of making a hyperbolic shaped reflector and its supporting structure. Both flat and hyperbolic BDLFR secondary reflectors have been compared. The results show that, for similar concentrations, the novel approach presents higher optical efficiency than the hyperbolic BDLFR. This result encourages the future integration of the flat BDLFR technology with industrial processes.

CRediT authorship contribution statement

Sebastián Taramona: Conceptualization, Methodology, Writing – review & editing. **Pedro Ángel González-Gómez:** Writing – original draft. **Javier Villa Briongos:** Visualization, Writing – review & editing. **Jesús Gómez-Hernández:** Supervision, Writing – review & editing.

Declaration of competing Interest

The authors declare that they have no known competing financial interests or personal relationships that could have appeared to influence the work reported in this paper.

Acknowledgements

The authors wish to thank the support for the research project INTECSOLARIS-CM-UC3M has been funded by the call “Programa de apoyo a la realización de proyectos interdisciplinares de I + D para jóvenes investigadores de la Universidad Carlos III de Madrid 2019–2020” under the frame of the “Convenio Plurianual Comunidad de Madrid - Universidad Carlos III de Madrid”.

The authors wish to thank “Comunidad de Madrid” for its support to the ACES2030-CM Project (S2018/EMT-4319) through the Program of R&D activities between research groups in Technologies 2018, co-financed by European Structural Funds.

Appendix A. Design chart consistency example

These figures, Figs. A1, A2 and A3 show the design charts for the solar field configurations presented in Table 1. Pointing out cases “A” and “B”:

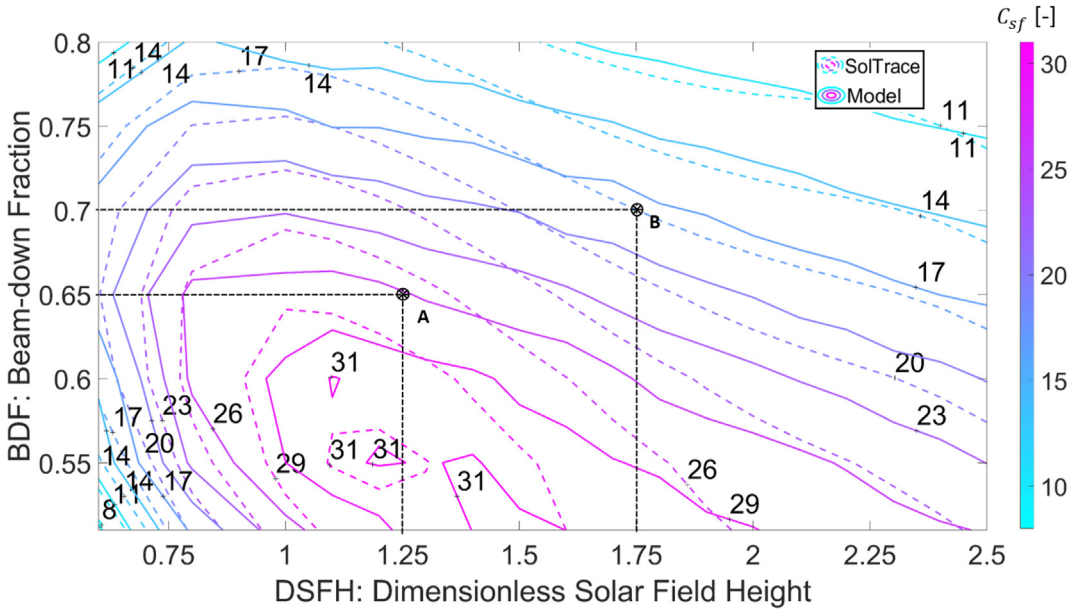

Fig. A1. Solar field concentration for cases A and B.

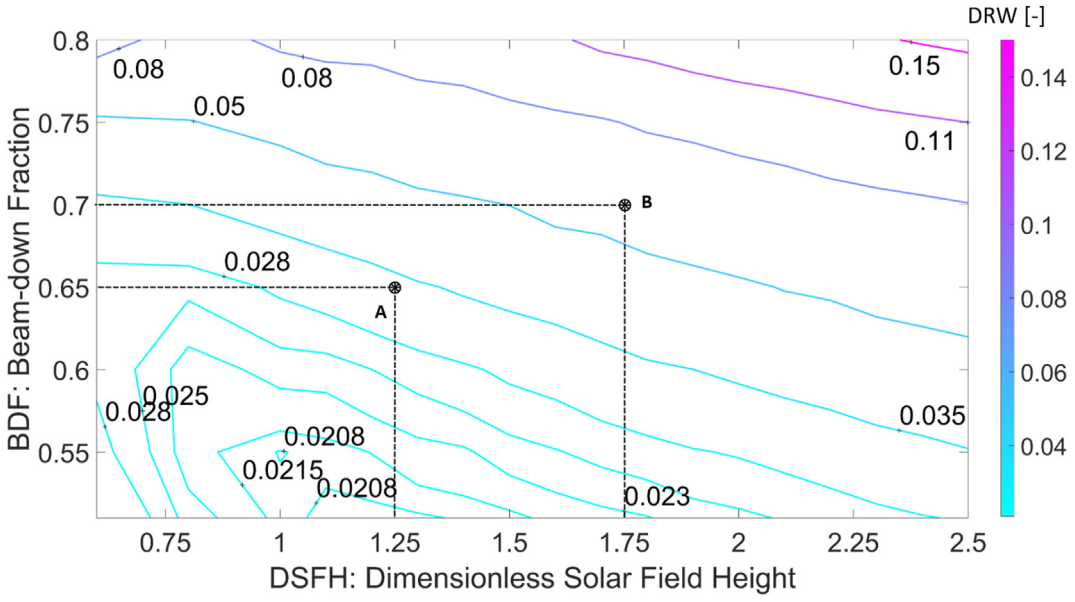

Fig. A2. Dimensionless receiver width for cases A and B.

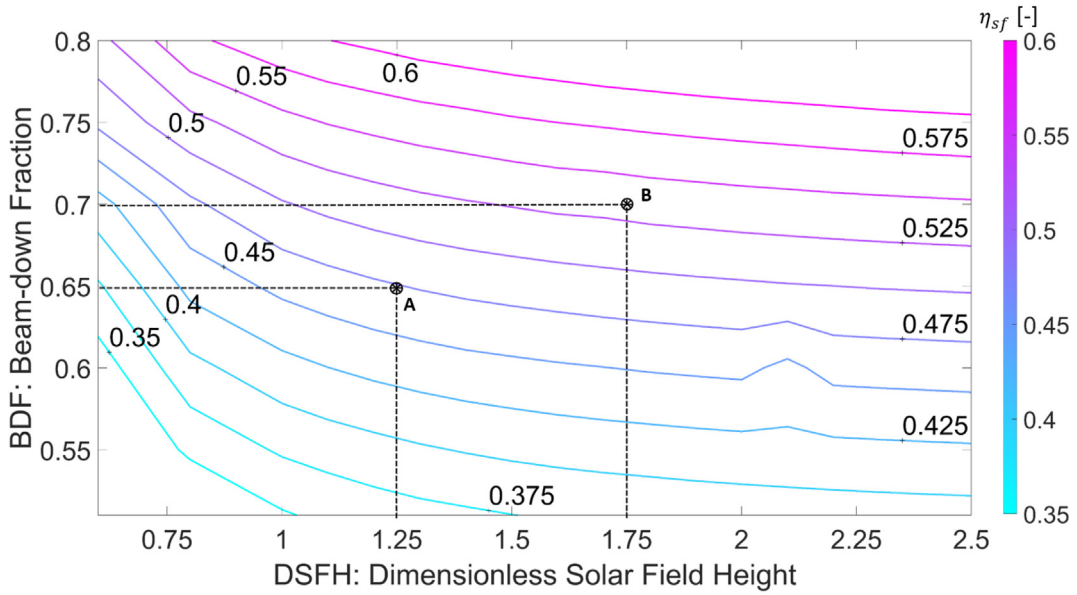

Fig. A3. Solar field efficiency for cases A and B.

Appendix B. Design chart use example

As a practical demonstration for the design charts benefits and ease of use, we are going to consider a realistic case as an example. For the hydrothermal carbonization of loblolly pine (one of the cases presented in Ref. [34]) a heat flux of 20 kW/m^2 is required, additionally we are going to consider that the mirror supplier only makes mirrors 0.5 m wide (w_m), and that the available space to locate our solar field is 25 m wide (w_{sf}).

- Assuming a Direct Net Irradiance of 1000 W/m^2, the required concentration of the field is $C_{sf} = 20$.
- The next thing is to determine the number of rows on each side of the receiver (N_r). Considering an extra space of 25% over the mirrors total width for the receiver width and the separation between mirrors, N_r can be obtained from: $2 \cdot w_m \cdot N_r \cdot 1.25 \leq w_{sf}$ resulting in $N_r = 20$.
- Limiting the space reserved for the distance between the mirrors to 10% of the total mirror width, the maximum receiver width can be calculated with the formula $(2 \cdot w_m \cdot N_r \cdot 1.1) + w_{rec} \leq w_{sf}$, which results in $w_{rec} \leq 3$ and DRW ≤ 0.3.
- For the maximum acceptable DRW value obtained, checking Fig. B3 it can be seen that all values of the design chart are viable, so to finish the design of the solar field the dimensionless parameter couple that maximizes the field efficiency are selected.
- Applying the $C_{sf} = 20$ curve over the efficiency chart, the couple of dimensionless parameters that result in the desired concentration with the maximum efficiency can be found, resulting in DSFH ~1.21 and BDF ~0.715.

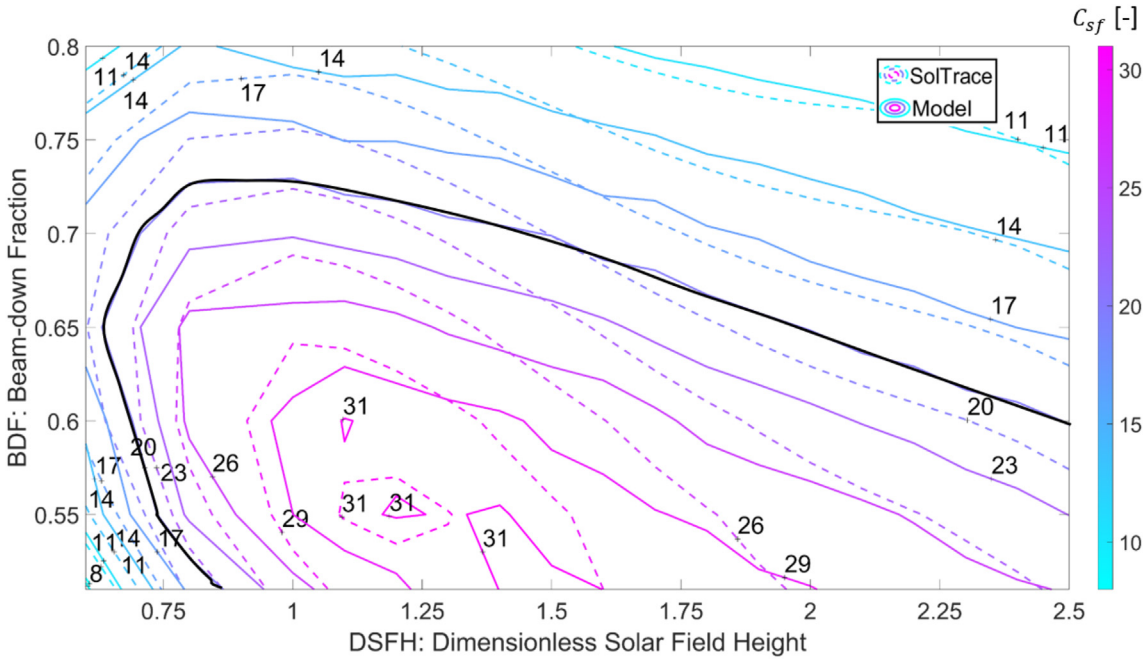

Fig. B1. Solar field concentration design chart with $C_{sf} = 20$ highlighted.

- With this pair of dimensionless parameters, the results obtained using the design charts are $C_{sf} = 20$, $\eta_{sf} = 53\%$ and DRW = 0.05.
- The solar field dimensions that fulfill all the requirements and restrictions are: $w_m = 0.5$ m, $N_r = 20$, $w_{rec} = 0.5$ m, $y_f = 12.1$ m and $y_{bd} = 8.652$ m.

The design charts used in this example are presented in Figs. B1 – B3.

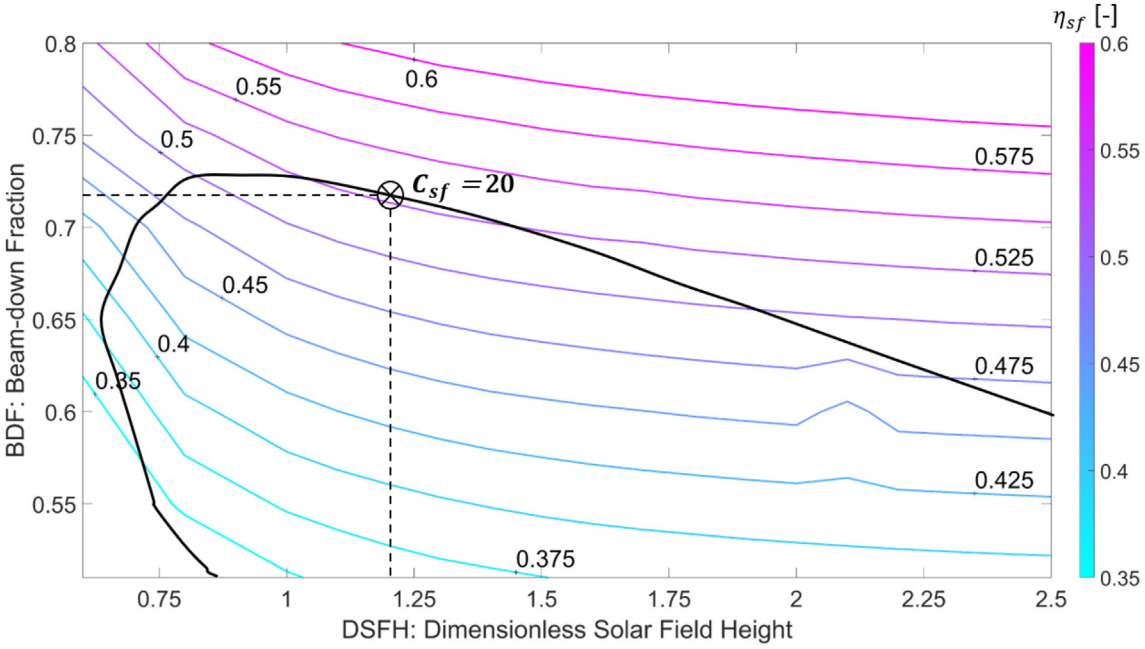

Fig. B2. Solar field efficiency design chart with $C_{sf} = 20$ and the maximum efficiency point overlayed.

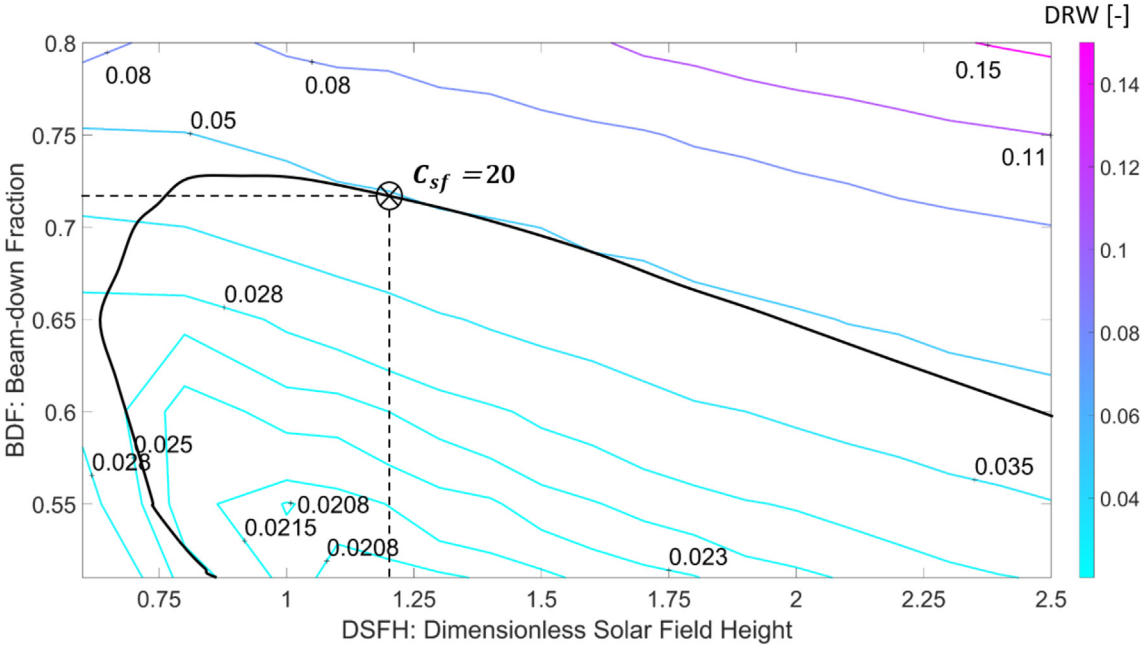

Fig. B3. Dimensionless receiver width design chart with $C_{sf} = 20$ and the maximum efficiency point overlayed.

References

[1] D. Santana, J. Gómez-Hernández, J. Villa Briongos, P.A. González-Gómez, Sistema óptico de haz descendente lineal solar, ES 2648148, A1, n.d.

[2] R. Abbas, M.J. Montes, M. Piera, J.M. Martínez-Val, Solar radiation concentration features in Linear Fresnel Reflector arrays, Energy Convers. Manag. 54 (2012) 133–144, https://doi.org/10.1016/j.enconman.2011.10.010.

[3] N. Kincaid, G. Mungas, N. Kramer, M. Wagner, G. Zhu, An optical performance comparison of three concentrating solar power collector designs in linear Fresnel, parabolic trough, and central receiver, Appl. Energy 231 (2018) 1109–1121, https://doi.org/10.1016/j.apenergy.2018.09.153.

[4] A.E. Rungasamy, K.J. Craig, J.P. Meyer, A review of linear Fresnel primary optical design methodologies, Sol. Energy 224 (2021) 833–854, https://doi.org/10.1016/j.solener.2021.06.021.

[5] R. Abbas, J.M. Martínez-Val, Analytic optical design of linear Fresnel collectors with variable widths and shifts of mirrors, Renew. Energy 75 (2015) 81–92, https://doi.org/10.1016/j.renene.2014.09.029.

[6] S. Benyakhlef, A. Al Mers, O. Merroun, A. Bouatem, N. Boutammachte, S. El Alj, H. Ajdad, Z. Erregueragui, E. Zemmouri, Impact of heliostat curvature on optical performance of Linear Fresnel solar concentrators, Renew. Energy 89 (2016) 463–474, https://doi.org/10.1016/j.renene.2015.12.018.

[7] D.R. Mills, G.L. Morrison, Compact linear fresnel reflector solar thermal powerplants, Sol. Energy 68 (2000) 263–283, https://doi.org/10.1016/S0038-092X(99)00068-7.

[8] A. Barbón, N. Barbón, L. Bayón, J.A. Otero, Theoretical elements for the design of a small scale Linear Fresnel Reflector: frontal and lateral views, Sol. Energy 132 (2016) 188–202, https://doi.org/10.1016/j.solener.2016.02.054.

[9] A. Barbón, N. Barbón, L. Bayón, J.A. Otero, Optimization of the length and position of the absorber tube in small-scale Linear Fresnel Concentrators, Renew. Energy 99 (2016) 986–995, https://doi.org/10.1016/j.renene.2016.07.070.

[10] N. Kincaid, G. Mungas, N. Kramer, G. Zhu, Sensitivity analysis on optical performance of a novel linear Fresnel concentrating solar power collector, Sol. Energy 180 (2019) 383–390, https://doi.org/10.1016/j.solener.2019.01.054.

[11] Y. Zhu, J. Shi, Y. Li, L. Wang, Q. Huang, G. Xu, Design and experimental investigation of a stretched parabolic linear Fresnel reflector collecting system, Energy Convers. Manag. 126 (2016) 89–98, https://doi.org/10.1016/j.enconman.2016.07.073.

[12] M.J. Montes, R. Abbas, M. Muñoz, J. Muñoz-Antón, J.M. Martínez-Val, Advances in the linear Fresnel single-tube receivers: hybrid loops with non-evacuated and evacuated receivers, Energy Convers. Manag. 149 (2017) 318–333, https://doi.org/10.1016/j.enconman.2017.07.031.

[13] S. Kiyaee, Y. Saboohi, A.Z. Moshfegh, A new designed linear Fresnel lens solar concentrator based on spectral splitting for passive cooling of solar cells, Energy Convers. Manag. 230 (2021) 113782, https://doi.org/10.1016/j.enconman.2020.113782.

[14] H. Zhai, Y.J. Dai, J.Y. Wu, R.Z. Wang, L.Y. Zhang, Experimental investigation and analysis on a concentrating solar collector using linear Fresnel lens, Energy Convers. Manag. 51 (2010) 48–55, https://doi.org/10.1016/j.enconman.2009.08.018.

[15] J. Gómez-Hernández, P.Á. González-Gómez, T. Ni-Song, J.V. Briongos, D. Santana, Design of a solar linear particle receiver placed at the ground level, AIP Conf. Proc. 2033 (2018) 2012–2016, https://doi.org/10.1063/1.5067169.

[16] J. Gómez-Hernández, P.A. González-Gómez, J.V. Briongos, D. Santana, Technical feasibility analysis of a linear particle solar receiver, Sol. Energy 195 (2020) 102–113, https://doi.org/10.1016/j.solener.2019.11.052.

[17] A. Sánchez-González, J. Gómez-Hernández, Beam-down linear Fresnel reflector: BDLFR, Renew. Energy 146 (2020) 802–815, https://doi.org/10.1016/j.renene.2019.07.017.

[18] A. Rabl, Tower reflector for solar power plant, Sol. Energy 18 (n.d.) 269.

[19] A. Segal, M. Epstein, The optics of the solar tower reflector, Sol. Energy 69 (2001) 229–241, https://doi.org/10.1016/s0038-092x(00)00137-7.

[20] A. Segal, M. Epstein, Comparative performances of “tower-top” and “tower-reflector” central solar receivers, Sol. Energy 65 (1999) 207–226, https://doi.org/10.1016/S0038-092X(98)00138-8.

[21] X. Li, M. Lin, Y. Dai, C.H. Wang, Comparison-based optical assessment of hyperboloid and ellipsoid reflectors in a beam-down solar tower system with linear fresnel heliostats, J. Sol. Energy Eng. Trans. ASME. 139 (2017) 1–14, https://doi.org/10.1115/1.4037742.

[22] A. Segal, M. Epstein, Practical considerations in designing large scale “beam down” optical systems, J. Sol. Energy Eng. 130 (2008) 19–20, https://doi.org/10.1115/1.2804629.

[23] L. Vant-Hull, Issues with beam-down concepts, Energy Proc. 49 (2014) 257–264, https://doi.org/10.1016/j.egypro.2014.03.028.

[24] M. Diago, N. Calvet, P.R. Armstrong, Net power maximization from a faceted beam-down solar concentrator, Sol. Energy 204 (2020) 476–488, https://doi.org/10.1016/j.solener.2020.04.061.

[25] T. Kodama, N. Gokon, K. Matsubara, K. Yoshida, S. Koikari, Y. Nagase, K. Nakamura, Flux measurement of a new beam-down solar concentrating system in Miyazaki for demonstration of thermochemical water splitting reactors, Energy Proc. 49 (2014) 1990–1998, https://doi.org/10.1016/j.egypro.2014.03.211.

[26] T. Kodama, et al., Particle reactors for solar thermochemical processes, Sol. Energy 156 (2017) 113–132, https://doi.org/10.1016/j.solener.2017.05.084.

[27] Y.T. Kodama, N. Gokon, H.S. Cho, K. Matsubara, H. Kaneko, K. Senuma, S. Itoh, Shin-nosuke, particles fluidized bed receiver/reactor tests with quartz sand particles using a 100-kW beam-down solar concentrating system at Miyazaki, AIP Conf. Proc. 1850 (2017) 1–9, https://doi.org/10.1063/1.4984469.

[28] T. Kodama, N. Gokon, S. Enomoto, S. Itoh, T. Hatamachi, Coal coke gasification in a windowed solar chemical reactor for beam-down optics, J. Sol. Energy Eng. 132 (2010) 1–6, https://doi.org/10.1115/1.4002081.

[29] C. Tregambi, P. Salatino, R. Solimene, F. Montagnaro, An experimental characterization of Calcium Looping integrated with concentrated solar power, Chem. Eng. J. 331 (2018) 794–802, https://doi.org/10.1016/j.cej.2017.08.068.

[30] A. Segal, M. Epstein, Solar ground reformer, Sol. Energy 75 (2003) 479–490, https://doi.org/10.1016/j.solener.2003.09.005.

[31] X. Li, Y.J. Dai, R.Z. Wang, Performance investigation on solar thermal conversion of a conical cavity receiver employing a beam-down solar tower concentrator, Sol. Energy 114 (2015) 134–151, https://doi.org/10.1016/j.solener.2015.01.033.

[32] N. Calvet, M. Martins, B. Grange, V.G. Perez, D. Belasri, M.T. Ali, P.R. Armstrong, N. Calvet, M. Martins, B. Grange, V.G. Perez, D. Belasri, M.T. Ali, P.R. Armstrong, The Masdar Institute Solar Platform: a new research facility in the UAE for development of CSP components and thermal energy storage systems, AIP Conf. Proc. 1734 (2016), https://doi.org/10.1063/1.4949191.

[33] M. Alqaydi, T. Delclos, S. Almheiri, N. Calvet, Effect of sand and method of Mixing on Molten salt properties for an open direct absorption solar receiver/storage system. https://doi.org/10.1063/1.4984423, 2017.

[34] J.V. Briongos, S. Taramona, J. Gómez-Hernández, V. Mulone, D. Santana, Solar and biomass hybridization through hydrothermal carbonization, Renew. Energy 177 (2021), https://doi.org/10.1016/j.renene.2021.05.146.

[35] V. Sharma, J.K. Nayak, S.B. Kedare, Effects of shading and blocking in linear Fresnel reflector field, Sol. Energy 113 (2015) 114–138, https://doi.org/10.1016/j.solener.2014.12.026.

[36] R. Winston, L. Jiang, V. Oliker, Nonimaging Optical Systems, Nonimaging Opt., 2020, pp. 47–72, https://doi.org/10.1201/9780429168246-4.

[37] S.S. Mathur, T.C. Kandpal, B.S. Negi, Optical design and concentration characteristics of linear Fresnel reflector solar concentrators—I. Mirror elements of varying width, Energy Convers. Manag. 31 (1991) 205–219, https://doi.org/10.1016/0196-8904(91)90075-T.

[38] T. Wendelin, A. Dobos, A. Lewandowski, SolTrace: a ray-tracing code for complex solar optical systems, Contract 303 (2013) 275–3000.

[39] J. Sun, Z. Zhang, L. Wang, Z. Zhang, J. Wei, Comprehensive review of line-focus concentrating solar thermal Technologies: parabolic trough collector (PTC) vs linear fresnel reflector (LFR), J. Therm. Sci. 29 (2020) 1097–1124, https://doi.org/10.1007/s11630-020-1365-4.

[40] G. Morin, J. Dersch, W. Platzer, M. Eck, A. Häberle, Comparison of linear fresnel and parabolic trough collector power plants, Sol. Energy 86 (2012) 1–12, https://doi.org/10.1016/j.solener.2011.06.020.

[41] R. Gabbrielli, P. Castrataro, F. Del Medico, M. Di Palo, B. Lenzo, Levelized cost of heat for linear Fresnel concentrated solar systems, Energy Proc. 49 (2014) 1340–1349, https://doi.org/10.1016/j.egypro.2014.03.143.